Numerical investigation on sealing performance of non-contact finger seal with herringbone groove surface topography

Numerical investigation on sealing performance of non-contact finger seal with herringbone groove surface topography

Lingping Chen[1,2], Yanchao Zhang[1*], Yahui Cui[1], Bowen Zhi[1], Jie Wang[1], Mingfeng Wang[3]

1. School of Mechanical and Precision Instrumental Engineering, Xi'an University of Technology, Xi'an, 710048, China
2. School of Mechanical Engineering, Hunan Institute of Engineering, Xiangtan, Hunan, 411104, China
3. Brunel University London, Department of Mechanical and Aerospace Engineering, London, UB8 3PN, United Kingdom

* Corresponding author: Yanchao Zhang, School of Mechanical and Precision Instrumental Engineering, Xi'an University of Technology, No. 5 Jinhua South Road, Beilin District, Xi'an, Shaanxi 710048, China; Email: zhangyanchao@xaut.edu.cn; Tel.: +86-135-7187-4962

Keywords: Non-contact finger seal, herringbone groove, surface topography, fluid-structure interaction, mixed-level uniform design method; correlation analysis

Abstract: Since the last decade, the non-contact finger seal (NCFS) has attracted an increasing number of researchers due to its inherent flexibility and non-contact features, which can significantly improve the service life and reduce the leakage rate of the finger seals. In this paper, to enhance the NCFS sealing performance, lifting pads with twenty (20) different herringbone groove surface topographies are proposed based on the uniform design method. Numerical analysis is carried out based on the two-way fluid-structure interaction (FSI) method to better mimic the actual working conditions. The analysis of results using statistical tools reveals that the herringbone groove topographies placed on the bottom surface of low-pressure lifting pads can significantly improve the load-carrying capacity and sealing performance. In addition, the correlation analysis of the sealing performance and geometric parameters of the herringbone groove demonstrate that reducing the groove width or increasing the groove internal angle can improve the lifting and leakage capacities. Finally, the optimal herringbone groove and general structure (no groove) are comparatively analysed under variable working conditions, and the results show that the former has much better sealing performance.

1. Introduction

As a compliant rotor seal, finger seals are well known for their low leakage rate and long service life, which makes them have great potential in the application of aero-engines and gas turbines [1,2]. Finger seals are classified into contact and non-contact finger seals (NCFSs). The friction and wear caused by the interference fit between the contact-type finger seal and the rotor adversely affect the service life of the finger seal [3,4]. In contrast, the fit between the NCFS and the rotor is a clearance fit. The NCFS is a combined hydrodynamic and hydrostatic seal with positive leakage. At the high rotation and the inlet/outlet pressure difference, a high-pressure gas film is formed between the rotor and the NCFS, which effectively reduces friction and wear [5]. Thus, NCFSs have attracted much attention.

At present, research on NCFSs has mainly focused on revealing their dynamic characteristics and performing numerical simulations of the fluid-structure interaction (FSI). Du *et al.* proposed a semi-analytical kinetic method to characterize the linear dynamic characteristics and leakage performance of an NCFS [6,7]. Cao *et al.* proposed a three-dimensional porous media model for leakage analysis of an NCFS and investigated the influence of the rotor speed, seal clearance, and pressure difference on the lifting characteristics of the NCFS [8]. Braun *et al.* designed a two-layer lifting pad structure for finger seal [9]. This structure takes advantage of the mutual extrusion of the two lifting pads to improve the

rebound ability of the finger beam and reduce the hysteresis of the finger seal. Furthermore, they also conducted comprehensive investigations of the one-way FSI of the NCFS [10,11]. The numerical flow field results (i.e., force) were applied to the structure solver to calculate structural parameters (e.g., displacement) of the finger seal, and some preliminary designs for NCFSs were proposed based on the one-way FSI method. However, they did not consider the real-time interaction between the structural and the flow field.

When the structure of the NCFS deforms, the flow field changes accordingly, which then affects the structural deformation [12]. Therefore, the flow field and deformation of the NCFS cannot be accurately simulated using the one-way FSI method. Conversely, in the two-way FSI analysis, the data exchange is bidirectional; that is, the results of the fluid analysis (i.e., force) are transferred to the structural analysis, and the results of the structural analysis (i.e., displacement) are transferred back to the fluid analysis [13,14]. Su *et al.* combined the two-way FSI numerical method with surface topography technology to investigate the sealing characteristics of an NCFS under working conditions [15,16]. Their research shows that processing a series of surface topographies on the surface of the rotor or the lifting pad is conducive to improving the sealing performance of the NCFS. Zhang *et al.* used two-way FSI to carry out a dynamic simulation analysis on an NCFS with grooved pads [17]. Compared with the general structure, the groove topography could effectively improve the sealing performance.

The above researches have made great contributions to the mechanical design and sealing performance improvement of the NCFS. However, further research is still needed to improve the hydrodynamic effect and the sealing performance of the NCFS. In recent years, numerous studies have shown that non-smooth surfaces have great potential in improving the lubrication and wear resistance of friction pairs [18–20]. Specifically, the main functions of surface textures/topographies can be classified into several types according to different lubrication states: (1) under mixed to dry friction, acting as traps to capture wear debris and reducing resistance and adhesion [21]; (2) under mixed to boundary lubrication, providing micro-reservoirs and resulting in numerous micro-fluid film bearings to enhance lubrication of friction pairs [22]; (3) under hydrodynamic lubrication, generating hydrodynamic pressure to increase the load-carrying capacity [23,24]. Among them, the main function mechanism of surface texture/topography under hydrodynamic lubrication can be explained as follows: In hydrodynamic lubrication, positive pressure will be generated when fluid flows along a convergent gap, but not along a divergent gap. The surface texture provides the regular convergence gap and divergence gap [22]. When the fluid film flows into the texture region, a divergence gap is formed, resulting in the decrease of fluid film pressure (even negative pressure) and cavitation once the negative pressure reaches a certain limit value; when the fluid film flows out the texture region, a convergence gap is formed, increasing fluid film pressure and resulting in a pressure peak region. Therefore, an asymmetric pressure distribution is generated in each micro-texture unit, which makes the fluid film capable of bearing a certain force.

Surface texture/ topography forms can be classified into pockets, dimples, textures, and grooves according to their geometric characteristics. Among them, herringbone groove structure is widely used in biomedical [25], chemistry [26], machinery [27], and other fields owing to its special geometric characteristics. Wang *et al.* proposed a new face seal with herringbone spiral groove and studied the gas film pressure distribution on the sealing surface through one-dimensional and two-dimensional numerical analyses. The results show that this new face seal has excellent bearing capacity and sealing performance [28]. Gao *et al.* studied the effect of herringbone groove on the performance of aerostatic sliding bearing by numerical analysis and experimental verification. The results show that the herringbone groove can significantly improve the performance of aerostatic journal bearing (e.g.,

improving the bearing capacity and reducing air consumption) [29]. Proctor *et al.* proposed a new NCFS, in which the straight groove and the herringbone groove were set on the lifting pad and the rotor respectively. The experimental results show that this new proposed NCFS has good sealing performance (its leakage rate is less than one-third of a straight four-tooth labyrinth seal at 5000 r/min of rotor speed and less than one-half of a contacting brush seal at static conditions) [30,31].

Motivated by encouraging results with herringbone grooves, an idea came to the minds of authors to conceive new herringbone grooved NCFS (combined with the application of straight groove and herringbone groove in [30,31]) for further improving the sealing performance. This paper is organized as follows: Section 2 constructs the geometric model and two-way FSI calculation model of the NCFS and then describes the uniform design of the herringbone groove and the validation of the numerical model compared to available experimental data [31]. Section 3 illustrates the numerical simulations result from the aspect of sealing performance analysis, performance parameter analysis, flow field analysis, and operating condition analysis. Section 4 comes to the conclusion that the proposed herringbone groove can significantly improve the sealing performance of the NCFS.

2. Model definition and verification

2.1. Geometric model of the NCFS

The basic structure of the NCFS includes 2~4 layers of high-pressure (HP) finger laminate, a low-pressure (LP) finger laminate, a front spacer, a front plate, and a back plate, as shown in Figure 1(a). The finger laminates are the most critical parts of an NCFS, placed in a staggered manner along the rotor axis. The number of laminates in a typical NCFS may vary between three to five. The HP finger laminate composes of a sealing annulus and a series of finger curved beams from the inner circle to the finger feet, as shown in Figure 1(b). Different from the HP finger laminate, the finger feet of the LP one are processed into lifting pads along the axial direction, as shown in Figure 1(c). At high-speed rotation of the rotor, a thin gas film between the finger feet and the rotor is formed. This gas film can help to meet the requirement of sealing function and avoid direct contact between the finger feet and the rotor, which reduces the wear and improves the service life of the NCFS significantly.

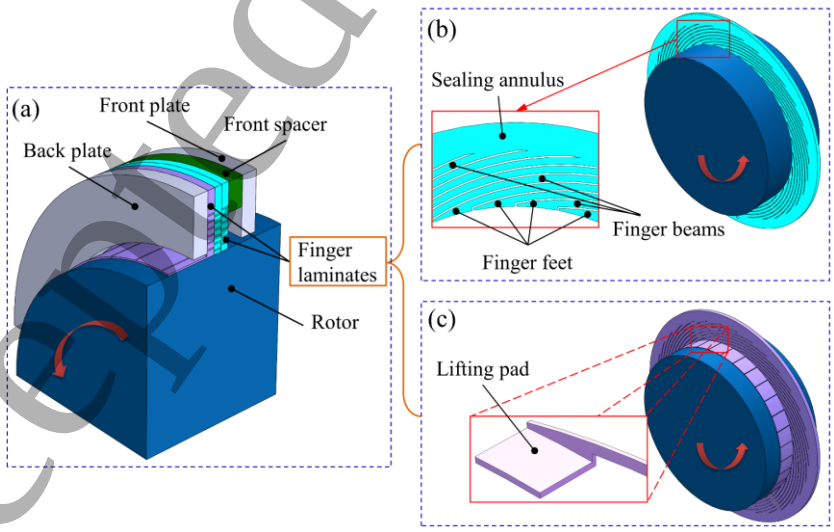

Figure 1. Diagram of non-contact finger seal (NCFS): (a) assembly sketch; (b) high-pressure (HP) finger laminate; (c) low-pressure (LP) finger laminate.

There are two main leakage channels in the finger seal, as shown in Figure 2: one is the clearance between the finger feet and rotor, which is called finger feet clearance (FFC); the other is the clearance

between the finger beams, which is called the finger clearance (FC). The finger laminates are staggered along the axis to prevent leakage caused by the circumferential clearance of the finger beam.

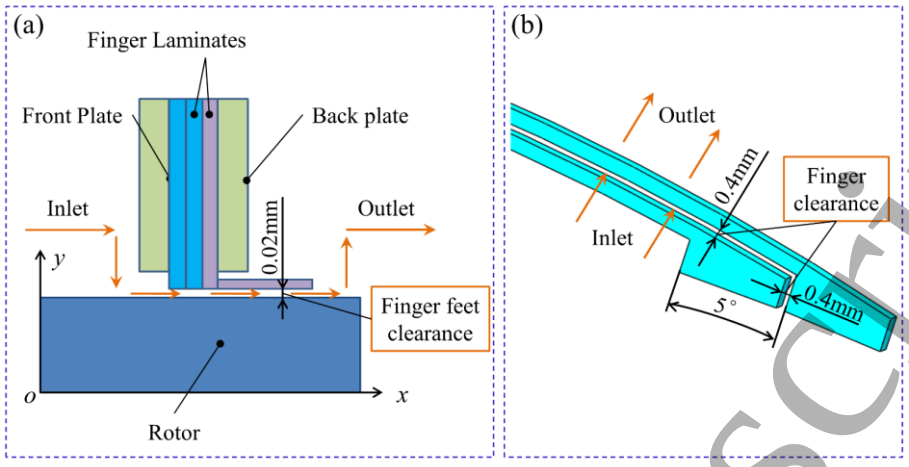

Figure 2. Leakage channels of the NCFS: (a) finger feet clearance (FFC); (b) finger clearance (FC).

2.2. Geometric model of the herringbone groove surface topography

To improve the sealing performance of the NCFS, herringbone groove surface topography is designed at the bottom of the LP lifting pad, as shown in Figure 3. In the structural diagram of the herringbone groove, *a* is the groove width, *b* is the groove length, *c* is the groove spacing, *d* is the groove margin, θ is the groove internal angle, and *h* is the groove depth. It has been reported in several studies that the geometric properties of surface topographies (such as spacing, arrangement, density, section geometric parameters, and depth) have a great impact on the tribological properties of two relatively sliding surfaces [32–34]. This paper focuses on the influence of section geometric parameters and depth of single-pair herringbone groove on the sealing performance of the NCFS.

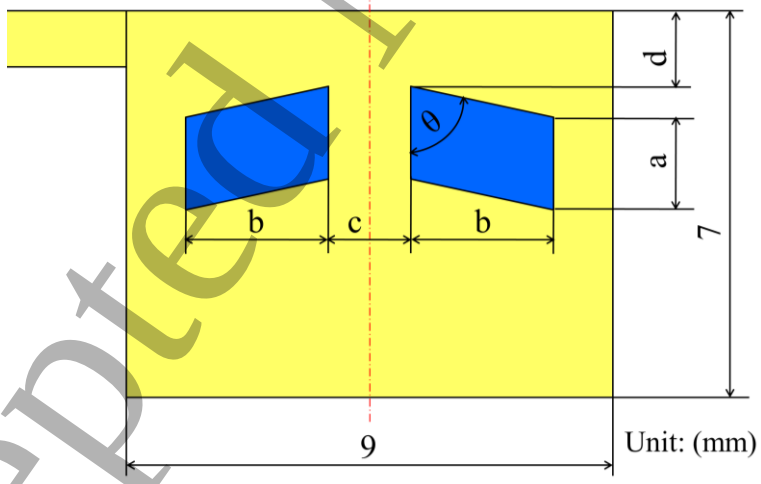

Figure 3. Structural diagram of the herringbone groove.

Considering the geometric complexity of the herringbone groove, a Uniform Design (UD) is employed to arrange the experiment and discover the synergistic effect of the herringbone groove geometric parameters on the finger sealing performance. UD experiment is a method established together by Fang Kaitai & academician Wang Yuan, which applies the experiments with many factors and many levels and is based on orthogonal test [35]. UD can distribute the experiment points evenly in the factor space to have fewer trails and each point has full representation [36]. When the levers of each factor are equal, the general UD table can be used, otherwise, the mixed level UD table should be adopted [37,38].

The general UD table can be expressed as $U_n(q^s)$, where U stands for uniform design, n for the number of trials, q for the number of levels, and s for the number of factors.

The UD experiment is performed using the software DPS (Data Processing System, Version 9.5, Zhejiang University, Hangzhou, China), which is the most popular multifunctional statistical analysis software with complete experimental design and statistical analysis functions in China [39]. DPS has outstanding performance in constructing large-scale UD and mixture design tables. In this paper, there are six experimental factors: a, b (b/a = 1.5), c, d, θ, and h. Three of these factors are assigned four levels and two factors of five levels, as listed in Table 1. As the levels of each factor are not the same, so the mixed level UD is adopted in this paper and the number of tests is set to 20 (20 = 4 × 5, the minimum number of tests is equal to the common multiple of the number of different levels), as listed in Table 2. For more detail about the framework of UD in this paper, see the flowchart of Figure 4.

Table 1. Parameter settings for the herringbone groove surface topography

Groove Factor	Level 1	Level 2	Level 3	Level 4	Level 5
Width, a (mm)	1.2	1.6	2	2.4	
Length, b (mm)	1.8	2.4	3	3.6	
Spacing, c (mm)	1.2	1.6	2	2.4	
Margin, d (mm)	0.5	1	1.5	2	
Internal angle, θ (°)	30	45	60	75	90
Depth, h (mm)	0.05	0.1	0.15	0.2	0.25

Table 2. Design parameters of the herringbone groove surface topography

Groove Factor	Width, a	Length, b	Spacing, c (mm)	Margin, d	Depth, h	Internal angle, θ (°)
N1	1.2	1.8	1.2	2	0.25	60
N2	1.6	2.4	1.6	2	0.05	60
N3	1.2	1.8	2	1.5	0.05	90
N4	1.2	1.8	1.6	1	0.1	30
N5	1.2	1.8	1.6	0.5	0.15	75
N6	2	3	2.4	1	0.05	60
N7	2.4	3.6	1.2	1.5	0.1	75
N8	2.4	3.6	2.4	2	0.1	30
N9	1.6	2.4	2	2	0.15	45
N10	2	3	1.2	1.5	0.15	30
N11	1.6	2.4	2	0.5	0.25	30
N12	2	3	1.2	0.5	0.05	45
N13	2.4	3.6	2	0.5	0.2	60
N14	2.4	3.6	1.6	1	0.25	45
N15	1.2	1.8	2.4	1.5	0.2	45
N16	2.4	3.6	2	1	0.15	90
N17	2	3	1.6	2	0.2	90
N18	1.6	2.4	1.2	1	0.2	90
N19	2	3	2.4	1.5	0.25	75
N20	1.6	2.4	2.4	0.5	0.1	75

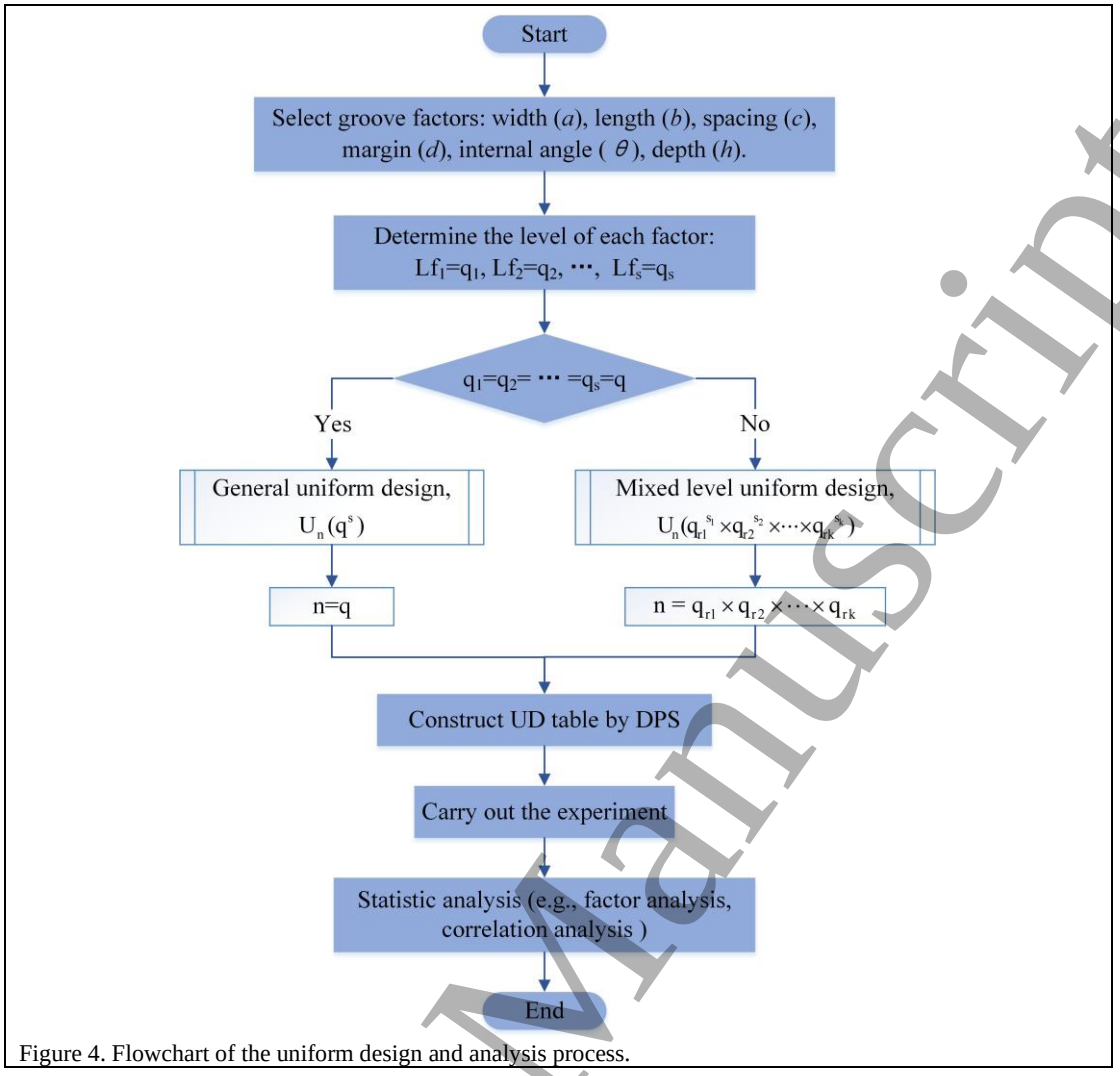

Figure 4. Flowchart of the uniform design and analysis process.

2.3. Calculation model and validation

2.3.1. Two-way FSI calculation model

In the two-way FSI calculation, owing to the highly cyclic symmetry of the NCFS structure, 1/72 of the entire seal structure is considered in the periodic calculation model to analyse the gas flow in detail. The solid model includes a complete LP laminate and two half (½) HP laminates. The fluid model includes the FC between the finger laminates and the FFC between the finger feet and the rotor. The fluid medium is air at room temperature. More details are shown in Figure 5, where the numbers represent different boundary conditions in the two-way FSI calculation, i.e., pressure (1), fixed support (2), fluid-solid interface (3), opening (4 and 5), symmetric (6 and 7), and rotating wall (8).

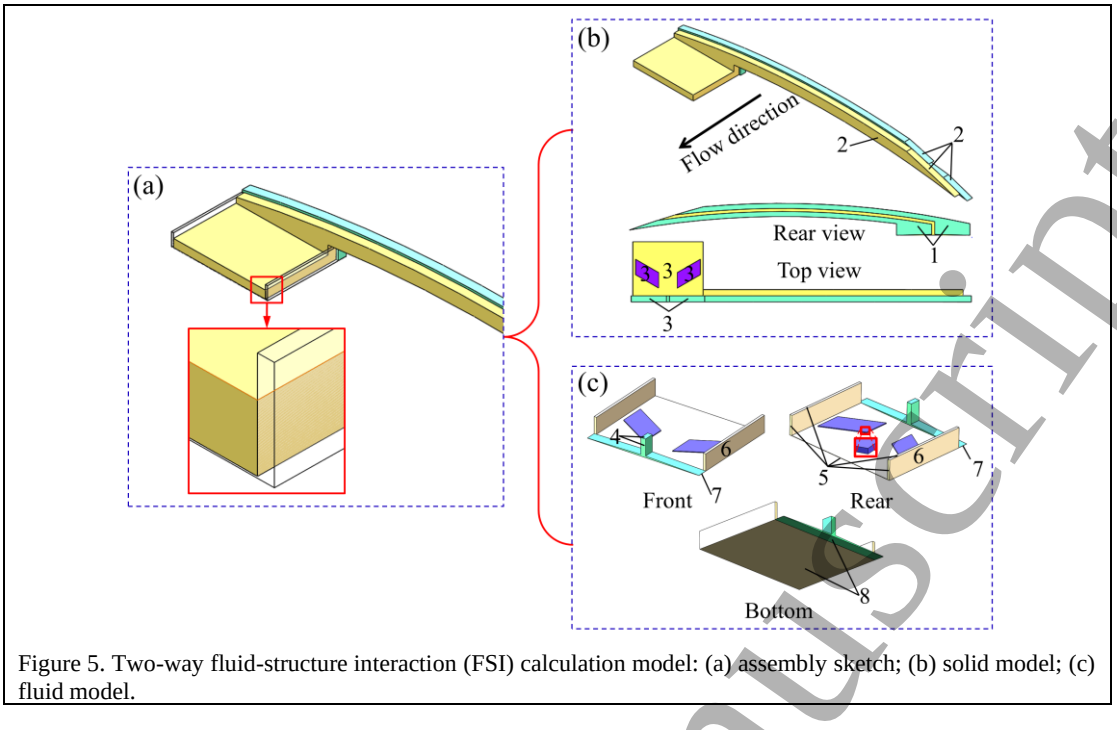

Figure 5. Two-way fluid-structure interaction (FSI) calculation model: (a) assembly sketch; (b) solid model; (c) fluid model.

2.3.2. Grid independence analysis

To reduce the calculation complexity, a grid quality independence test of the NCFS without herringbone groove (the general structure) is conducted before the formal numerical computations. The grid quality is controlled by adjusting parameters such as the element sizing and relevance. Taking the grid quality of the solid and fluid domains as variables and the leakage of the NCFS as the analysis objective, the influence of different grid qualities on the leakage is analysed.

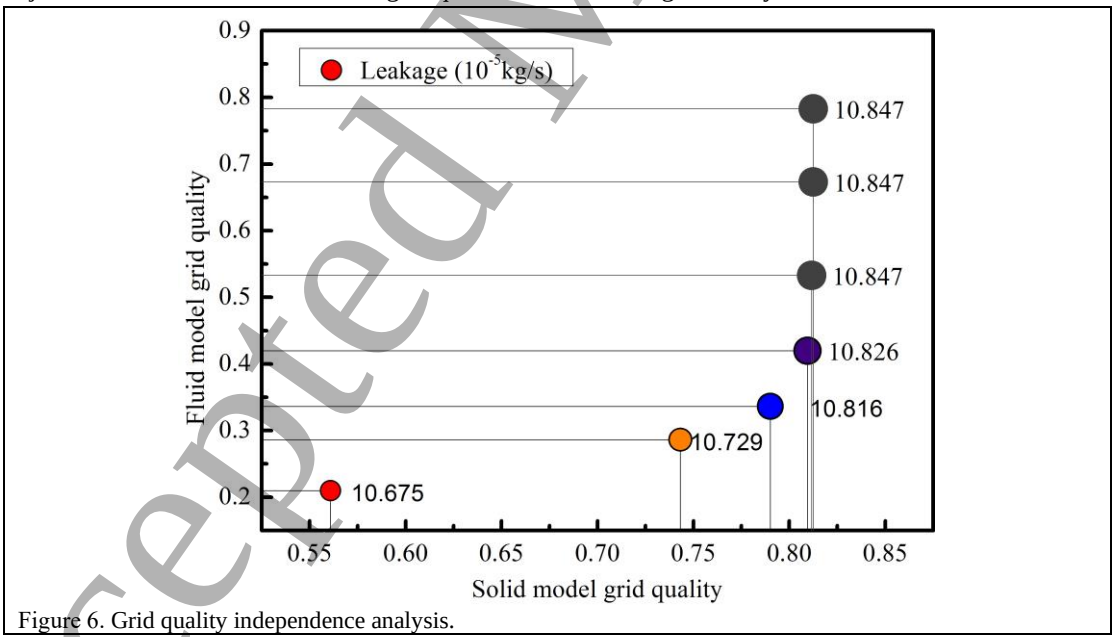

Figure 6. Grid quality independence analysis.

As shown in Figure 6, when the grid qualities of the solid and fluid domains are below a value of 0.809 and 0.419, respectively, the leakage rate corresponding to different grid qualities varies significantly. When the solid grid quality is 0.812 and the fluid grid quality is 0.532, the leakage rate is 10.847×10^{-5} kg/s; however, once the grid qualities exceed these values, the leakage value remains the same, and it can be considered that the calculation result is independent of the grid quality. In this case,

the element sizing of the solid and fluid domains is set to 0.1 mm, and the relevance is set to 40%. For the herringbone structure, the facing sizing is set to 0.025 mm. Notably, the calculation model is meshed using the Auto Grid method in ANSYS Workbench. For regular geometry, the system automatically gives priority to the scanning division method, using hexahedral elements, otherwise tetrahedral elements. Furthermore, prisms and pyramids are required in the transition of this hybrid mesh. Take the 5th herringbone groove as an example, after meshing, the grids contain Tetrahedrons (number of elements: 476287)–Hexahedrons (103488)–Pyramids (736)–Wedges (224), and the obtained computation grids are shown in Figure 7.

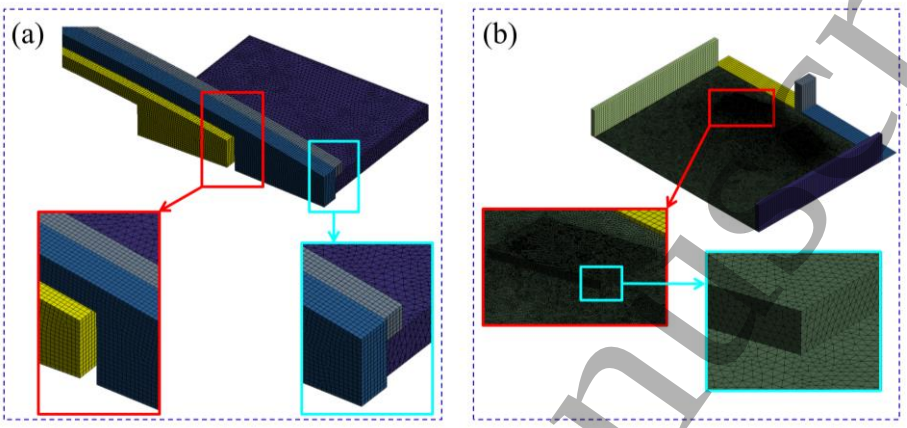

Figure 7. Periodic computation grids: (a) solid domain grid and (b) fluid domain grid.

2.3.3. Numerical calculation method

The two-way FSI method is employed for the numerical analysis of the NCFS. Two types of discretization techniques are used: the finite element method (FEM) is used for the structural mechanics, while the finite volume method (FVM) is used for the fluid zone calculations. It should be noted that the structural and flow modelling are performed in the Mechanical module and CFX module of ANSYS, respectively. At the same time, data is transmitted between the two modules by the fluid-structure interface, where fluid nodes must be mapped to the structural elements to transfer FEM results (i.e., displacements), and vice-versa [40]. Moreover, the commonly used turbulence models in the CFX software are the k-ε model and the shear stress transport (SST) model. The SST model has high accuracy in the transfer calculation of turbulence. It considers the turbulent shear stress and does not over-predict the eddy viscosity. In this study, the SST model is employed for the solution.

2.3.4. Validation of the numerical approach and model

For the experiments with the NCFS, the representative study by Proctor is used as a reference. In that study, Proctor conducted static and dynamic tests on an NCFS with a herringbone grooved rotor and acquired detailed and credible test data [31]. To verify the accuracy of the numerical model in this study, the same numerical model as in [31] is established, and the two-way FSI calculation is carried out under the same boundary conditions as the experimental values. Finally, the calculation results are compared with the test data. The leakage parameter of the test in [31] is given in the form of a flow factor, which is defined in equation (3):

$$\phi = \frac{\dot{m}\sqrt{T_{avg}}}{P_u D_{seal}} \tag{1}$$

where $\dot{m}$ is the mass flow rate through the entire flow field, T_{avg} is the average temperature at the inlet of the finger seal, P_u is the pressure at the inlet of the finger seal, and D_{seal} is the rotor diameter. The unit of the flow factor is kg·K$^{1/2}$/(MPa·m·s). A group of dynamic test data is employed for comparison with the numerical simulation results, as shown in Figure 7. In the numerical calculation, according to the operating parameters of the experiment in [31], the temperature is 300 K, rotating speed is 5000 r/min, assembly clearance between the finger feet and rotor is 25.4 μm, and the pressure differences are 13.8, 34, 69, 103, 138, 176, 207, and 241 kPa. The flow factors calculated by the simulation are consistent with the overall trend of the experimental results in [31].

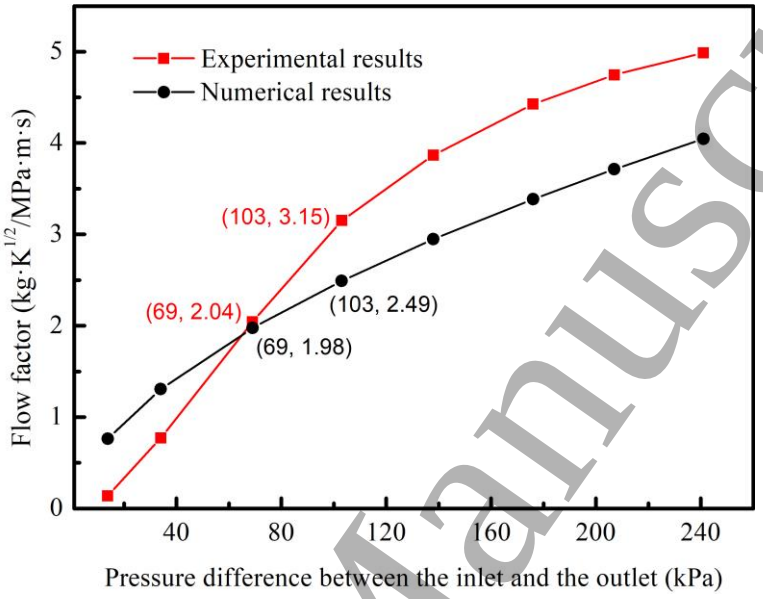

Figure 8. Comparison of the numerical results obtained with the proposed model and the experimental results in [31].

As shown in Figure 8, with the increasing pressure difference between the inlet and outlet, the leakage factor increases significantly when the pressure difference is less than 103 kPa (i.e. LP) and more gradually when the pressure difference is greater than 103 kPa (i.e. HP). This is mostly because when the pressure difference is sufficiently large, the finger seal starts to deform axially, resulting in the phenomenon of "holding the rotor", and the leakage clearance between the finger feet and the rotor decreases, resulting in a slower leakage rate. Moreover, the simulation results are lower than the experimental results when the pressure difference is more than 69 kPa. The main reasons are as follows: (1) uncontrollable factors (e.g. the assembly state and leakage channel) may cause a smaller leakage factor at the beginning of the test; (2) the simulation model only considers two types of leakage (i.e. FC leakage and FFC leakage), while the actual test also includes a third type (i.e. side clearance leakage), which causes a smaller leakage factor in the simulation; (3) the actual leakage in the test process will be greater owing to the temperature effect, rotor vibration, and other uncontrollable factors. Furthermore, the simulation value is approximately 80% of the experimental value when the pressure difference is more than 103 kPa, which is also consistent with the previous finding that the leakage path of the NCFS mainly consists of FFC leakage and FC leakage. Therefore, the accuracy and reliability of the two-way FSI method and turbulence model are verified.

3. Numerical simulations and results

3.1. Sealing performance analysis

There is no doubt that the leakage rate has a significant impact on the stability and effectiveness of the NCFS. Furthermore, the hydrodynamic pressure film formed between the rotor and the lifting pad should have sufficient bearing capacity to ensure the non-contact state of the NCFS during actual operation. Therefore, the leakage rate and the gas film force are the most important indexes of the sealing performance of the NCFS. In the case of hydrodynamic lubrication, the thinner fluid film produces a larger hydrodynamic bearing force [41]. The tribological properties between the NCFS and the rotor belong to hydrodynamic lubrication. Therefore, the larger gas film force calculated in this paper corresponds to the smaller gas film thickness and lower leakage rate, as shown in Figure 9(b), in which the sample points in the blue frames represent the preferred sealing performance.

As shown in Figure 9(a), the total leakage of the NCFS without herringbone groove is 10.847×10^{-5} kg/s, and the FFC leakage is 4.083×10^{-5} kg/s. For the NCFS with herringbone grooves, in the 20 groups of uniform experiment samples, the total leakages are all considerably reduced compared with the general structure. Except for the 10th and 16th test samples, in which the FFC leakages are slightly higher than that of the general structure, all the FFC leakages decreased considerably in the other 18 groups of test samples. This indicates that the herringbone groove can effectively reduce the leakage of the finger seal. Furthermore, it is easy to see that the leakage results of the 8th, 10th, 13th, and 16th test samples are not satisfactory. In practice, the reason for these results is that these herringbone grooves are beyond the lifting pads, as shown in Figure 10. In this case, a large amount of fluid flows out along the groove, resulting in the increase of leakage rate and the decrease of gas film force. Therefore, this situation should be avoided in the design of the herringbone groove.

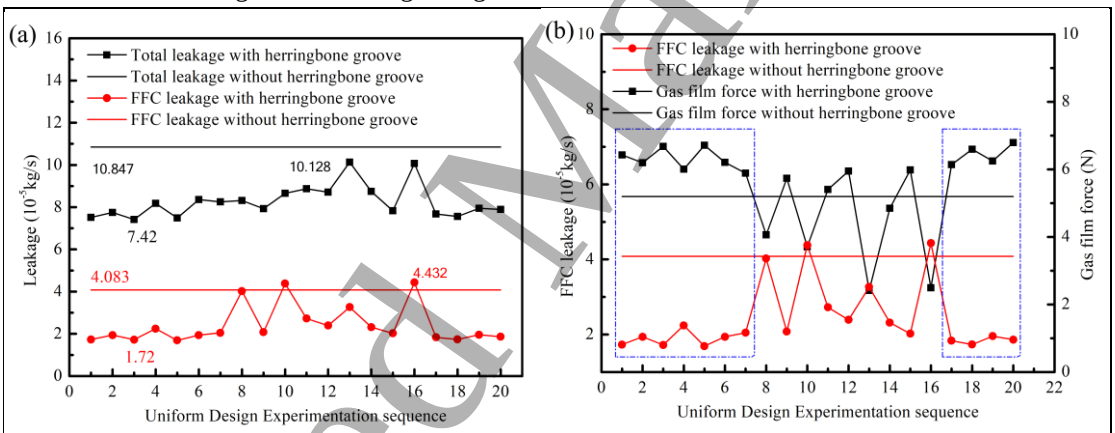

Figure 9. Leakage and Gas film force: (a) total leakage and FFC leakage and (b) gas film force.

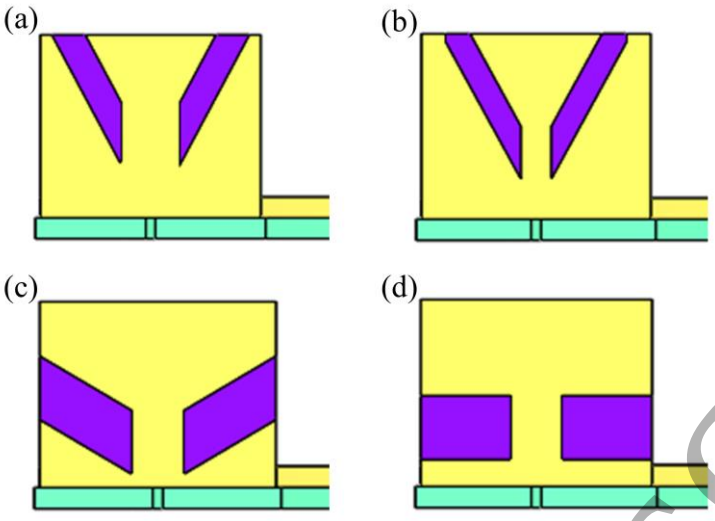

Figure 10. Four herringbone grooves exceeding the lifting pads: (a) N8; (b) N10; (c) N13; (d) N16.

3.2. Performance parameter analysis

The simulation data for the 20 types of NCFS with herringbone grooves are summarised in Table 3, where $\dot{m}$ is the total leakage rate, $\dot{m}_f$ is the FFC leakage rate, F is the gas film force, and $\dot{m}_f/\dot{m}$ is the ratio of FFC leakage to total leakage, ΔF is the increment change in the gas film force relative to the general structure, and $\nabla\dot{m}$, $\nabla\dot{m}_f$, $\nabla(\dot{m}_f/\dot{m})$ are the decrements of the total leakage, FFC leakage, and $\dot{m}_f/\dot{m}$, respectively. To improve the sealing performance of the NCFS, it is necessary to increase the gas film force and reduce the total leakage, FFC leakage, and contribution of the FFC leakage to the total leakage. Based on the data for ΔF, $\nabla\dot{m}$, $\nabla\dot{m}_f$, and $\nabla(\dot{m}_f/\dot{m})$, the Statistical Product and Service Solutions (SPSS) system [42] and factor analysis method are used to calculate the comprehensive scores of the 20 types of NCFS, as indicated in the last column of Table 3. For the convenience of visualization, the data in Table 3 are arranged in descending order according to the comprehensive scores. The comprehensive score of the 5th herringbone groove is the highest (0.920), reflecting the outstanding sealing performance of the NCFS (the gas film force is 23.98% higher than that of the general structure, and the FFC leakage is 58.59% lower). However, the comprehensive score of the 16th herringbone groove is the lowest (-2.313), reflecting the inferior sealing performance of the NCFS (the gas film force is 42.86% lower than that of the general structure, and the FFC leakage is 8.54% higher).

Table 3. Simulation data for NCFS with herringbone groove surface topographies

Number	$\dot{m}$ (10^{-5}kg/s)	$\dot{m}_f$ (10^{-5}kg/s)	F(N)	ΔF	$\nabla\dot{m}$	$\nabla\dot{m}_f$	$\nabla(\dot{m}_f/\dot{m})$	Score
N5	7.485	1.691	7.040	23.98%	30.99%	58.59%	40.00%	0.920
N3	7.420	1.72	7.010	23.45%	31.60%	57.87%	38.41%	0.908
N18	7.562	1.734	6.934	22.12%	30.29%	57.55%	39.10%	0.843
N1	7.511	1.73	6.784	19.48%	30.75%	57.65%	38.83%	0.831
N20	7.896	1.863	7.110	25.22%	27.21%	54.37%	37.32%	0.706
N17	7.679	1.834	6.525	14.91%	29.21%	55.08%	36.55%	0.660
N2	7.751	1.939	6.575	15.80%	28.54%	52.51%	33.55%	0.546
N19	7.944	1.956	6.624	16.65%	26.76%	52.10%	34.61%	0.528
N15	7.831	2.021	6.385	12.46%	27.80%	50.51%	31.45%	0.440

Number	$\dot{m}$ (10^{-5}kg/s)	$\dot{m}_f$ (10^{-5}kg/s)	F(N)	ΔF	$\nabla\dot{m}$	$\nabla\dot{m}_f$	$\nabla(\dot{m}_f/\dot{m})$	Score
N9	7.927	2.078	6.160	8.49%	26.92%	49.11%	30.36%	0.381
N6	8.363	1.937	6.588	16.02%	22.89%	52.57%	38.49%	0.371
N7	8.254	2.046	6.297	10.90%	23.90%	49.90%	34.16%	0.365
N4	8.177	2.242	6.402	12.76%	24.61%	45.09%	27.17%	0.225
N12	8.711	2.39	6.354	11.90%	19.69%	41.47%	27.12%	0.020
N14	8.743	2.317	5.361	-5.58%	19.40%	43.27%	29.61%	-0.230
N11	8.874	2.725	5.860	3.21%	18.19%	33.28%	18.46%	-0.380
N10	8.656	4.379	4.338	-23.60%	20.20%	-7.24%	-34.37%	-1.205
N8	8.313	4.023	4.654	-18.04%	23.36%	1.48%	-28.55%	-1.476
N13	10.128	3.266	3.171	-44.16%	6.63%	20.02%	14.34%	-2.140
N16	10.065	4.432	3.245	-42.86%	7.21%	-8.54%	-16.97%	-2.313
No groove	10.847	4.083	5.678					

In addition, the SPSS system is adopted to analyse the correlation between the sealing performance parameters of the NCFS and the structural parameters of the herringbone groove. As indicated in Table 4, the total leakage and FFC leakage are significantly positively correlated with the groove width (the correlation coefficients are 0.721 and 0.628, respectively) and negatively correlated with the groove internal angle (the correlation coefficients are -0.448 and -0.576, respectively). In contrast, the gas film force is significantly negatively correlated with the groove width (the correlation coefficient is -0.667) and positively correlated with the groove internal angle (the correlation coefficient is 0.497). This illustrates that the total leakage and FFC leakage increase with increasing groove width and decrease with increasing groove internal angle, while the variation in the gas film force is exactly the opposite to the leakage. Therefore, a herringbone groove with a smaller groove width and larger groove internal angle is more conducive to improving the sealing performance of the NCFS. Besides the groove width and groove internal angle, the other structural parameters of the herringbone groove have little effect on the sealing performance of the NCFS.

Table 4. Correlation tests based on the Spearman rank correlation coefficient

		Width, a	Spacing, c	Margin, d	Angle, θ	Depth, h
$\dot{m}$	Correlation coefficient	0.721**	0.124	-0.403	-0.448*	0.086
	Significance	0	0.602	0.078	0.048	0.719
$\dot{m}_f$	Correlation coefficient	0.628**	0.078	-0.132	-0.576**	0.049
	Significance	0.003	0.745	0.58	0.008	0.837
F	Correlation coefficient	-0.667**	0.016	-0.016	0.497*	-0.166
	Significance	0.001	0.948	0.948	0.026	0.485

**The correlation is significant at the 0.01 level (two-tailed).

*The correlation is significant at the 0.05 level (two-tailed).

3.3. Flow field analysis

The flow field between the finger feet and the rotor is analysed by drawing surface streamlines on the interface for further investigation. Several groups of herringbone groove samples exhibiting superior and inferior sealing performance in Table 3 are employed for comparative analysis with the general structure, and the surface streamlines are shown in Figures 11–13. In Figures 11–13 several common characteristics can be identified. (1) From the inlet HP zone to the outlet LP zone, the velocity of the fluid decreases correspondingly. (2) Owing to the influence of the rotor rotation, the flow velocity on the left side of the interface is slightly higher than that on the right side. (3) There are two high-speed flow

regions on both sides of the connection between the HP and LP zones, with a speed of approximately 550 m/s. This high-speed phenomenon is caused by the jet produced by the fluid entering the FFC from the FC. Compared with the FFC, the size of the FC is enormous, and their connection area is similar to that of a duck nozzle structure, which results in a high-speed flow area. (4) In the middle of the HP zone, there is a low-speed flow area, and the flow velocity is close to 0 m/s. This phenomenon is attributed to the formation of vortices in the FC, which create counteracting flow velocities in different directions, resulting in a low average velocity.

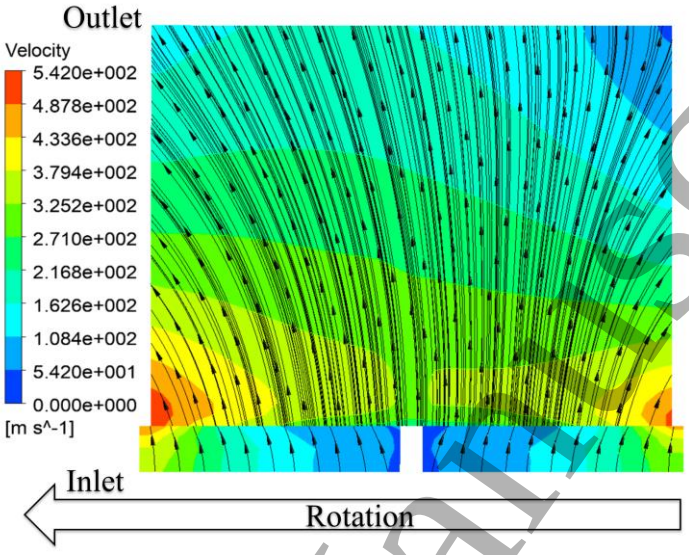

Figure 11. Surface streamlines of the interface without herringbone grooves.

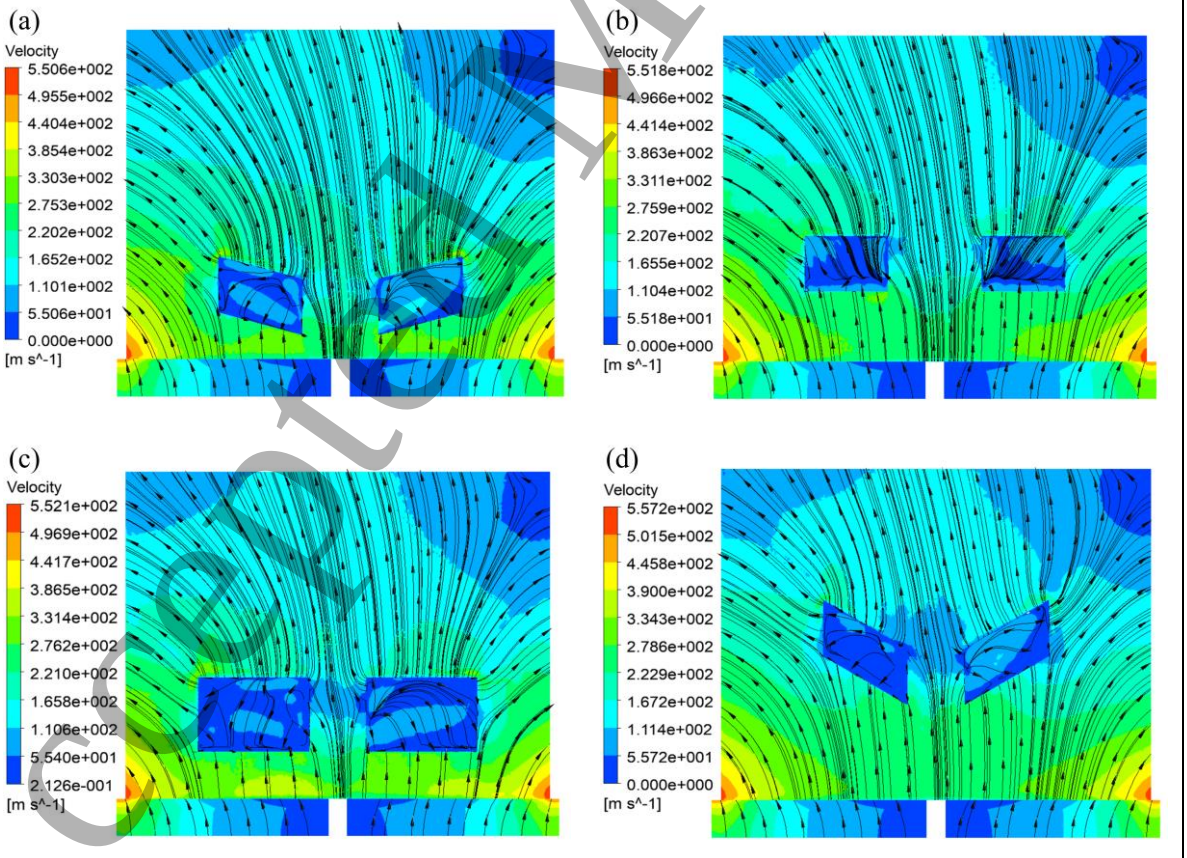

Figure 12. Surface streamlines of herringbone groove interfaces with superior sealing performance: (a) N5; (b) N3; (c)

N18; (d) N1.

The surface streamlines for four herringbone groove interfaces that demonstrated superior sealing performance are shown in Figure 12. There is an obvious circumfluence in the herringbone groove zone, which is caused by the vortices generated by the flow in the herringbone groove. When the fluid flows through the herringbone groove, a large amount of fluid flows into the herringbone groove owing to the sharp change in the local boundary. However, when the fluid flows out of the herringbone groove, its boundary forms a local obstacle. Thereby, the internal structure of the fluid generates dissociation and vortices, resulting in the bending of the streamlines and changes in the velocity distribution. This in turn increases the relative motion of the fluid, generates pressure resistance, and causes local head loss. Finally, the total mechanical energy of the fluid drops suddenly, reducing the flow velocity and leakage of the axial clearance. Therefore, as shown in Figure 12 after the fluid passes through the herringbone groove, the flow rate drops significantly. The vortices in the herringbone groove cause the flow velocities in different directions to counteract each other, and thus the average velocity is very low. Furthermore, the vortices can exert a major radial lifting force on the lifting pads. The vortex lift is the fundamental reason that the herringbone groove can provide a greater gas film force for the NCFS.

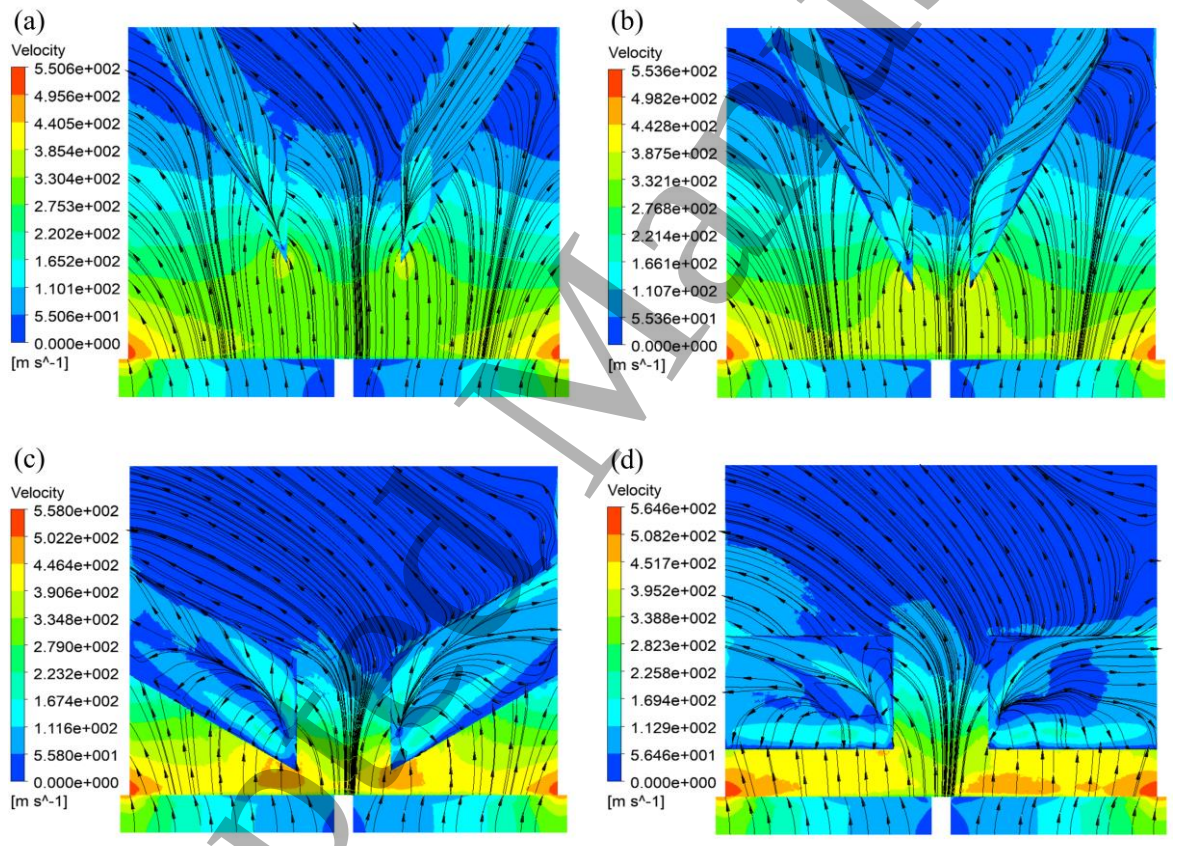

Figure 13. Surface streamlines of herringbone groove interfaces with inferior sealing performance: (a) N8; (b) N10; (c) N13; (d) N16.

The surface streamlines for four herringbone groove interfaces that demonstrated inferior sealing performance are shown in Figure 13. As the herringbone groove exceeds the bottom of the lifting pad, when the fluid passes through the herringbone groove, a large amount of fluid flows into the groove and along the groove to the outlet or FC, thus increasing the leakage. In this instance, the herringbone groove is equivalent to a diversion structure. Furthermore, the smaller groove margin makes the herringbone groove as close to the HP zone as possible, thereby increasing the slow-down area correspondingly after

the fluid passes through the herringbone groove. Therefore, under the influence of the rotor speed, the streamlines with lower velocity deflect strongly in the axial direction, thus reducing the axial leakage.

3.4. Operating condition analysis

To verify the adaptability of the herringbone groove designed in this study under different operating conditions, comparative analyses are carried out between the 5th herringbone groove and the general structure without grooves. As shown in Figure 14, when the assembly clearance (20 μm) and the pressure difference (0.3 MPa) are constant, the sealing performance of the 5th groove is significantly better than that of the general structure at different linear velocities of the rotor. The decrease in the total leakage, $\nabla\dot{m}$, is 30.89%, and the increase in the gas film force, ΔF, is 21.49%. These results are similar to the results in Table 3, thus reflecting the effectiveness of the herringbone groove under variable rotation conditions.

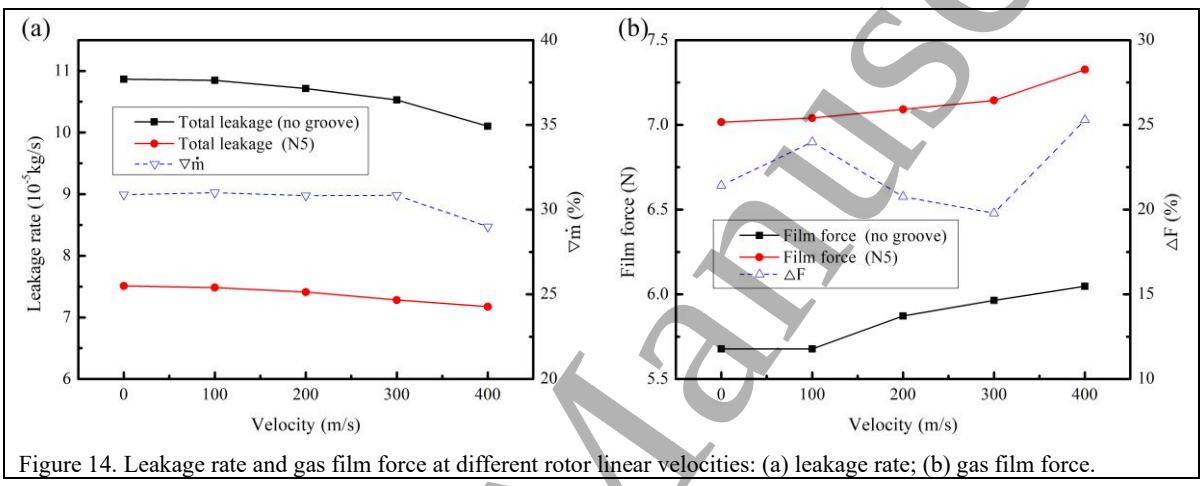

Figure 14. Leakage rate and gas film force at different rotor linear velocities: (a) leakage rate; (b) gas film force.

Figure 15 shows the surface limit streamlines and pressure of the 5th herringbone groove under the static state and a rotor linear velocity of 400 m/s. As mentioned before, the NCFS is a combined hydrodynamic and hydrostatic seal with positive leakage. When the rotor is stationary, the pressure and limit streamline on the interface are symmetrically distributed (see Figure 15(a-b)). It should be noted that in case of no groove, there is only the hydrostatic effect of the inlet/outlet differential pressure, while in the case of herringbone groove (e.g., N5), there are both hydrostatic and hydrodynamic effects (see the circumfluence and uneven pressure distribution of the herringbone groove in Figure 15(a-b)). It can be inferred that the herringbone groove is conducive to the hydrodynamic effect, and the specific reason analysis is the same as in Section 3.3. When the rotor rotates, there is no doubt that there are both hydrodynamic and hydrostatic effects, and the pressure and the limit streamlines on the interface are asymmetrically distributed. Moreover, the larger the rotor linear velocity is, the more obvious this asymmetric distribution will be (see Figure 15(c-d)).

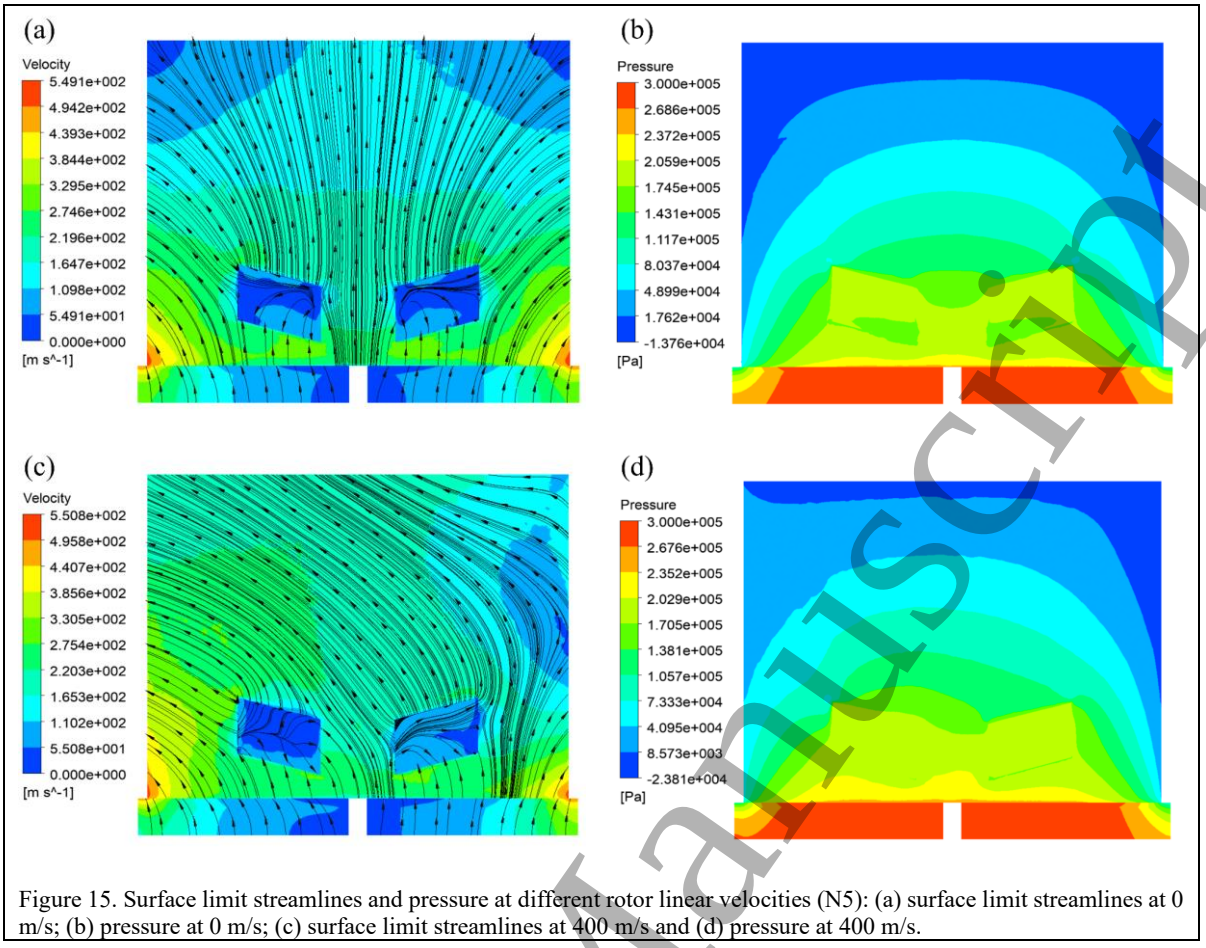

Figure 15. Surface limit streamlines and pressure at different rotor linear velocities (N5): (a) surface limit streamlines at 0 m/s; (b) pressure at 0 m/s; (c) surface limit streamlines at 400 m/s and (d) pressure at 400 m/s.

As shown in Figure 15, when the assembly clearance (20 μm) and rotor linear velocity (100 m/s) are constant, the sealing performance of the 5th herringbone groove is better than that of the general structure at varying pressure differences. Moreover, the larger the pressure difference is, the more obvious the performance advantage of the 5th herringbone groove will be.

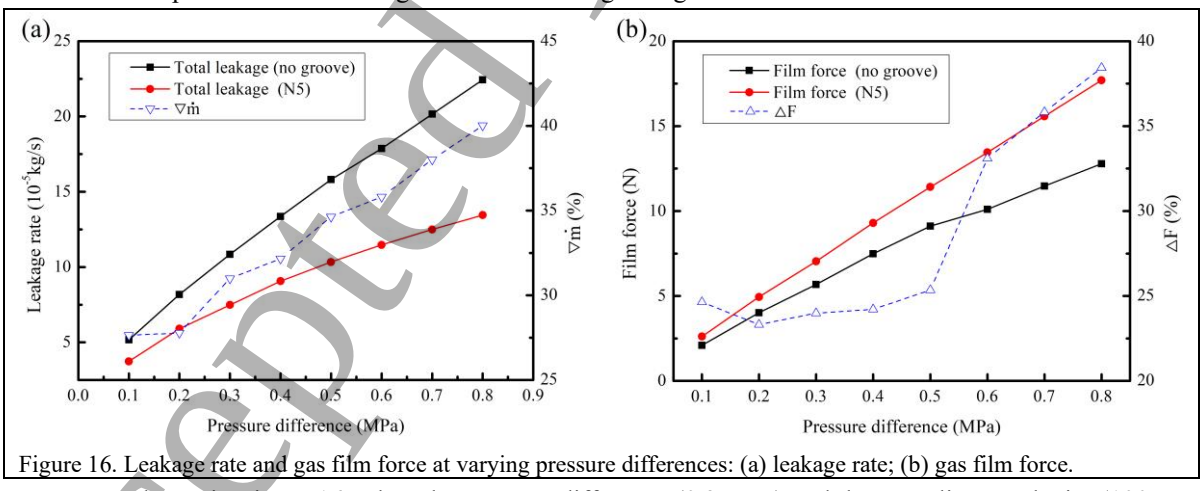

Figure 16. Leakage rate and gas film force at varying pressure differences: (a) leakage rate; (b) gas film force.

As shown in Figure 16, when the pressure difference (0.3 MPa) and the rotor linear velocity (100 m/s) are constant, the sealing performance of the 5th herringbone groove is better than that of the general structure at different assembly clearances. However, with an increase in the assembly clearance, the leakage rate of the two structures increases sharply, while the decrement of the total leakage, $\nabla\dot{m}$, and the gas film force decrease significantly. When the assembly clearance is 60 μm, $\nabla\dot{m}$ is only 9.57%, and the sealing performance advantage of the 5th herringbone groove is no longer obvious.

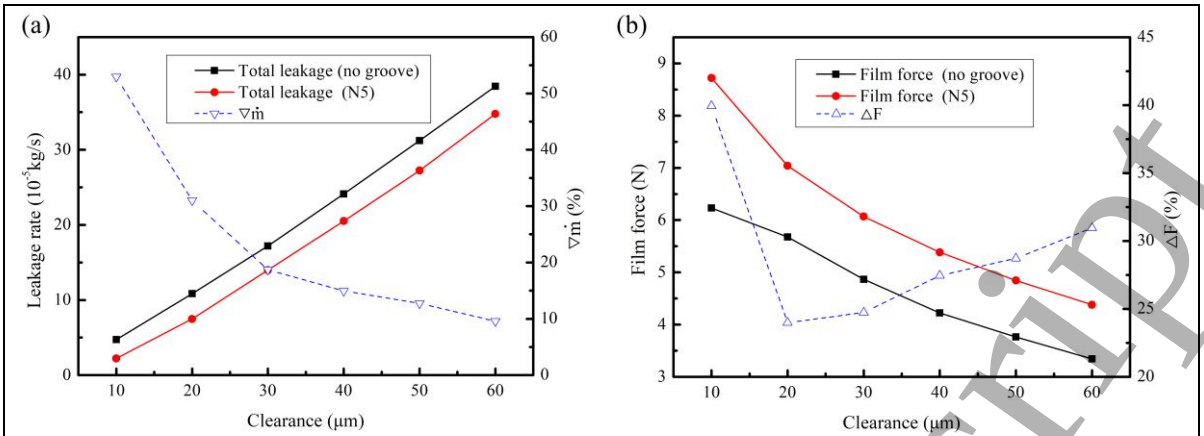

Figure 17. Leakage rate and gas film force at different assembly clearances: (a) leakage rate; (b) gas film force.

4. Conclusion

In this work, twenty (20) types of herringbone groove surface topographies have been designed at the lifting pad of non-contact finger seal (NCFS), and the effects of herringbone groove on the sealing performance of NCFS have been investigated by the numerical modelling and statistical analysis. The results have indicated that the geometrical characteristics of herringbone textures have a significant effect on the sealing performance of NCFS and the main conclusions are listed as follows:

1. Reasonable herringbone grooves (e.g., N5, N3, N18, and N1 in this study) can significantly improve the gas film force and reduce the leakage rate of the NCFS. The improvement of the gas film force is conducive to ensuring the non-contact state of the NCFS under adverse conditions and protecting the finger feet from the risk of wear. In addition, it is worth noting that configurations in which the herringbone groove exceeds the lifting pad should be avoided.

2. The total leakage and FFC leakage are significantly positively correlated with the groove width and negatively correlated with the groove internal angle. However, the gas film force exhibits the opposite trends to those of the leakage. Therefore, a herringbone groove with a smaller groove width and larger groove internal angle is optimal for improving the sealing performance. The 5th herringbone groove, which has the smallest groove width and groove margin and second-largest groove internal angle, exhibits the best sealing performance (the gas film force is 23.98% higher than that of the general structure, and the FFC leakage is 58.59% lower).

3. The vortices in the herringbone groove contribute significantly to the increase in the gas film force and decrease in the leakage. This provides a feasible way to improve the sealing performance by controlling the vortices in the sealing clearance. Furthermore, a smaller groove margin is conducive to broadening the low-speed area, which increases the axial deflection of the streamline to reduce axial leakage.

4. When the rotor linear velocity varies from 0 to 400 m/s, the pressure difference varies from 0.1 to 0.8 MPa, and the assembly clearance varies from 10 to 60 μm, the sealing performance of the 5th herringbone groove is significantly better than that of the general structure without grooves.

In future work, we will give further research about the effect of geometric properties of multi-pair herringbone grooves (e.g., spacing, arrangement, and density) on the sealing performance of the NCFS.

Declaration of Conflicting Interests

The author(s) declare no potential conflicts of interest with respect to the research, authorship, and/or publication of this article.

Acknowledgment

The author(s) would like to acknowledge the financial support received from the National Natural Science Foundation of China (Grant Nos. 52075436, 51305343) and the Education Department of Shaanxi Province (Grant No. 19JC030).

Nomenclature

a	Groove width	mm
b	Groove length	mm
c	Groove spacing	mm
d	Groove margin	mm
θ	Groove internal angle	°
h	Groove depth	mm
P	Pressure	Pa
$\dot{m}$	Mass flow rate	kg/s
$\dot{m}_f$	Finger feet clearance leakage rate	kg/s
F	Gas film force	N
Δ	Increment	-
∇	Decrement	-

Abbreviations

FSI	Fluid-structure interaction
HP	High pressure
LP	Low pressure
FFC	Finger feet clearance
FC	Finger clearance
SST	Shears stress transport
FEM	Finite element method
FVM	Finite volume method

References

[1] Wang L N, Chen G D, Su H, Lu F and Zhang Y C 2017 Effect of work status on leakage and contact pressure of C/C composite finger seal *Proc. Inst. Mech. Eng. Part C-Journal Mech. Eng. Sci.* **231** 925–40

[2] Chen L, Zhang Y, Cui Y, Wang J and Wang M 2021 Effect of snake-biomimetic surface texture on finger sealing performance under hydrodynamic lubrication *Surf. Topogr. Prop.* **9** 1–14

[3] Zhang Y C, Yin M H, Zeng Q R, Wang T and Wang R 2020 Theoretical and Experimental Investigation of Variable Stiffness Finger Seal *Tribol. Trans.* **63** 634–46

[4] Zhang Y C, Si C G, Zhang Y T, Zhang D Y and Cui Y H 2019 Effect of wear-resistant coatings on the comprehensive performance of finger seal *Proc. Inst. Mech. Eng. Part J-Journal Eng. Tribol.* **233** 570–9

[5] Zhang Y C, Wang T, Zhang D Y, Yin M H, Cui Y H, Chen L P, Du P F and Wang R 2020 Performance Analysis of Hydrodynamic Pressure Finger Seal by Wall Slip Effect *Math. Probl. Eng.* **2020** 14

[6] Du K, Li Y, Suo S and Wang Y 2015 Dynamic Leakage Analysis of Noncontacting Finger Seals Based on Dynamic Model *J. Eng. Gas Turbines Power* **137**

[7] Du K, Li Y, Suo S and Wang Y 2015 Semi-Analytical Dynamic Analysis of Noncontacting Finger Seals *Int. J. Struct. Stab. Dyn.* **15**

[8] Cao J, Jin F, Hu Y and Ji H 2014 Numerical Simulation on Lifting-force Characteristics of Finger Seal with Lifting-pads *Lubr. Eng.* **39** 52-56,62

[9] Braun M J, Marie H and Smith I 2010 Double padded finger seal ed P U S P 7735833 *P. U.S. Pat. 7735833* **Patent 77**

[10] Braun M J, Pierson H M and Kudriavtsev V V 2003 Finger Seal Solid Modeling Design and Some Solid/Fluid Interaction Considerations *Tribol. Trans.* **46** 566–75

[11] Braun M J and Li H 2008 An integrated numerical fluid/solid interaction model for finger seals with a padded low-pressure laminate *2007 ASME/STLE Int. Jt. Tribol. Conf. IJTC 2007* **PART A** 245–7

[12] Zhang H, Zheng Q and Yue G 2010 Study on the leakage and deformation characteristics of the finger seals by using numerical simulation *ASME Turbo Expo 2010: Power for Land, Sea, and Air, GT 2010* vol 4 (Glasgow, United kingdom: Proceedings of the ASME Turbo Expo) pp 1179–90

[13] Jia X Y, Zheng Q, Tian Z T, Jiang Y T and Zhang H 2018 Numerical investigations on lifting and flow performance of finger seal with grooved pad *Aerosp. Sci. Technol.* **81** 225–36

[14] Peters R D, van der Spuy S J, Els D N J and Kuhnert J 2018 Aerodynamic damping of an oscillating fan blade: Mesh-based and meshless fluid structure interaction analysis *J. Fluids Struct.* **82** 173–97

[15] Lu W and Su H 2015 Analysis of Structure and Performance of Finger Seal Combined with Circumferential Convergent Boots and Herringbone-groove *Mech. Sci. Technol. Aerosp. Eng.* **34** 1641–7

[16] Su H, Lang D and Qi F 2012 Structural Parameters Sensitivity Analysis of Hydrodynamic Finger Seal with Herringbone-grooved Rotor Based on Fuzzy Valuation *Lubr. Eng.* **37** 7–12

[17] Zhang H, Chai B Q, Jiang B, Zheng Q and Yue G Q 2015 Numerical Analysis of Finger Seal with Grooves on Lifting Pads *J. Propuls. Power* **31** 805–14

[18] Lu P and Wood R J K 2020 Tribological performance of surface texturing in mechanical applications—a review *Surf. Topogr. Metrol. Prop.* **8**

[19] Sharma N, Verma R, Sharma S and Kango S 2021 Qualitative potentials of surface textures and coatings in the performance of fluid-film bearings: a critical review *Surf. Topogr. Metrol. Prop.* **9**

[20] Pattnayak M R, Pandey R K and Dutt J kumar 2021 Performance improvement of an oil-lubricated journal bearing using bionic-textures fused micro-pockets *J. Tribol.* 1–32

[21] Korpela T, Suvanto M and Pakkanen T T 2012 Friction and wear of periodically micro-patterned polypropylene in dry sliding *Wear* **289** 1–8

[22] Pattnayak M R, Pandey R K and Dutt J K 2021 Effects of new micro-pocketed bore surface topographies on the performance behaviours of aerodynamic journal bearing *Surf. Topogr. Prop.* **9** 18

[23] Koutsoumpas G, Charitopoulos A, Papadopoulos C I and Fillon M 2020 Computational evaluation of dynamic coefficients of thrust bearings; effect of artificial texturing on thermohydrodynamic performance *Surf. Topogr. Metrol. Prop.* **8**

[24] Tala-Ighil N and Fillon M 2015 A numerical investigation of both thermal and texturing surface effects on the journal bearings static characteristics *Tribol. Int.* **90** 228–39

[25] Whulanza Y, Utomo M S and Hilman A 2017 Realization of Passive Micromixer using Herringbone Structure *2nd International Symposium of Biomedical Engineering (ISBE)* vol 1933 (Bali, INDONESIA: Amer Inst Physics)

[26] Chen X Y and Wang X L 2015 Optimized Modular Design and Experiment for Staggered Herringbone Chaotic Micromixer *Int. J. Chem. React. Eng.* **13** 305–9

[27] Ramesh A, Akram W, Mishra S P, Cannon A H, Polycarpou A A and King W P 2013 Friction characteristics of microtextured surfaces under mixed and hydrodynamic lubrication *Tribol. Int.* **57** 170–6

[28] Wang Y M, Yang H X, Wang J L, Liu Y M, Wang H N and Feng X Z 2009 Theoretical Analyses and Field Applications of Gas-Film Lubricated Mechanical Face Seals with Herringbone Spiral Grooves *Tribol. Trans.* **52** 800–6

[29] Gao S Y, Shi Y G, Xu L S, Chen H and Cheng K 2019 Investigation on influences of herringbone grooves for the aerostatic journal bearings applied to ultra-high-speed spindles *Proc. Inst. Mech. Eng. Part C-Journal Mech. Eng. Sci.* **233** 5795–812

[30] Proctor M P 2016 Non-contacting finger seals static performance test results at ambient and high temperatures *52nd AIAA/SAE/ASEE Joint Propulsion Conference, 2016, July 25, 2016 - July 27, 2016* (Salt Lake City, UT, United states: American Institute of Aeronautics and Astronautics Inc, AIAA)

[31] Proctor M P and Delgado I R 2008 Preliminary Test Results of a Non-Contacting Finger Seal on a Herringbone-Grooved Rotor *44th AIAA/ASME/SAE/ASEE Jt. Propuls. Conf. Exhib.* 1–23

[32] Senin N, Macaulay G, Giusca C and Leach R K 2014 On the characterisation of periodic patterns in tessellated surfaces *Surf. Topogr. Metrol. Prop.* **2**

[33] Huang W, Jiang L, Zhou C X and Wang X L 2012 The lubricant retaining effect of micro-dimples on the sliding surface of PDMS *Tribol. Int.* **52** 87–93

[34] Liu W, Ni H, Chen H and Wang P 2019 Numerical simulation and experimental investigation on tribological performance of micro-dimples textured surface under hydrodynamic lubrication *Int. J. Mech. Sci.* **163**

[35] Luo D 2012 Optimization of total polysaccharide extraction from Dioscorea nipponica Makino using response surface methodology and uniform design *Carbohydr. Polym.* **90** 284–8

[36] Shen G, Lu Y and Hong J 2006 Combined effect of heavy metals and polycyclic aromatic hydrocarbons on urease activity in soil **63** 474–80

[37] Lin C J and Jeng S Y 2020 Optimization of Deep Learning Network Parameters Using Uniform Experimental Design for Breast Cancer Histopathological Image Classification *Diagnostics* **10** 662–72

[38] Pan F and Zhu P 2011 Design optimisation of vehicle roof structures: benefits of using multiple surrogates *Int. J. Crashworthiness* **16** 85–95

[39] Tang Q Y and Zhang C X 2013 Data Processing System (DPS) software with experimental design, statistical analysis and data mining developed for use in entomological research *Insect Sci.* **20** 254–60

[40] Benra F K, Dohmen H J, Pei J, Schuster S and Wan B 2011 A comparison of one-way and two-way coupling methods for numerical analysis of fluid-structure interactions *J. Appl. Math.* **2011** 1–16

[41] Yao J, Chen L, Xia S, He J, Li C and Xiong Y 2019 Stability Analysis of Hydrodynamic Lubrication of a Liquid Conducting Film at Rail–Armature Interface *IEEE Trans. Plasma Sci.* **47** 2250–5

[42] Zhang Y J, Du Y X, Yu T, Feng Z J and Chen J Q 2019 Investigation of dextrin-based synergistic system with chiral ionic liquids as additives for enantiomeric separation in capillary electrophoresis *J. Pharm. Biomed. Anal.* **164** 413–20